ACS Catalysis

Research Article

pubs.acs.org/acscatalysis

Improving the Hydrogenation Function of Pd/γ-Al_2O_3 Catalyst by Rh/γ-Al_2O_3 Addition in CO_2 Methanation at Low Temperature

Alejandro Karelovic* and Patricio Ruiz

Institute of Condensed Matter and Nanosciences − Molecules, Solids and Reactivity (IMCN/MOST), Université catholique de Louvain, Croix du Sud 2/17, L7.05.15, 1348 Louvain-La-Neuve, Belgium

ABSTRACT: Catalytic CO_2 methanation at mild conditions ($T \leq 200$ °C) was studied over catalysts prepared by mechanically mixing in different proportions Rh(2 wt %)/γ-Al_2O_3 and Pd(5 wt %)/γ-Al_2O_3 catalysts. It was found that although Pd/γ-Al_2O_3 is inert at these conditions, the activity of the mechanical mixtures was up to 50% higher than that of the pure Rh/γ-Al_2O_3 catalyst. At 200 °C, with a H_2/CO_2 ratio of 4, the rate of reaction was 0.218×10^{-2} $mol_{CH_4}/mol_{Rh}/s$ for pure Rh/γ-Al_2O_3 catalyst and increased to 0.318×10^{-2} $mol_{CH_4}/mol_{Rh}/s$ for a catalyst containing 50 wt % of each catalyst, showing that a synergistic effect operates. In all cases, the selectivity to methane was 100%. No changes in the Rh oxidation state due to the presence of Pd/γ-Al_2O_3 after pretreatment and reaction was observed. A slight sintering of both metallic particles was observed. The presence of one catalyst did not affect the sintering of the other. No indication of migration of one metal to the surface of the other catalyst that can lead to the formation of bimetallic structures in the mixtures was observed. The nature and reactivity of reaction intermediates was studied by in situ DRIFTS performed at steady state and transient mode. Rh carbonyl hydride was the most abundant carbon-containing species adsorbed on Rh, whereas bridge-bonded CO dominated Pd sites. The reactivity of carbonyl species toward H_2 was greatly influenced by the relative proportions of Pd/γ-Al_2O_3 and Rh/γ-Al_2O_3 in the mixtures. Pd/γ-Al_2O_3 alone cannot hydrogenate the adsorbed CO species, whereas the presence of Rh/γ-Al_2O_3 significantly increased the reactivity of Pd−CO species, which is proposed to account for the observed synergistic effect. The analysis of apparent activation energies and H_2 and CO_2 reaction orders supports the suggestion that CO_2 is dissociated over both Pd and Rh and that the resulting CO(ads) species react to form methane aided by H species originating from Rh/γ-Al_2O_3 catalyst. Results show that a nominally inactive catalyst in CO_2 methanation, such as Pd/γ-Al_2O_3, can give rise to active surface species and produce methane with high selectivity when contacted with an appropriate promoter, such as Rh/γ-Al_2O_3.

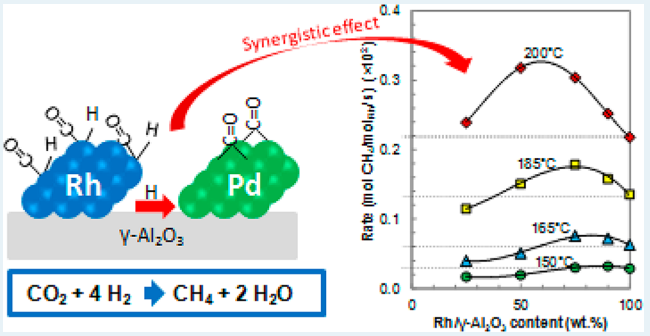

KEYWORDS: *CO_2 methanation, in situ DRIFTS, rhodium, palladium, Al_2O_3, bimetallic catalysts, low temperature, hydrogenation, kinetics, mechanical mixtures, spillover*

1. INTRODUCTION

One of the main challenges in heterogeneous catalysis is to perform reactions with high selectivity and reducing energetic consumption.[1] This can be achieved by performing processes under mild reaction conditions (low temperature and low pressure). The transformation of CO_2 into useful products is one of the major challenges in the development of environmentally friendly and sustainable processes.[2,3] The recycling of CO_2 to fuels or raw materials that are consumed in large scale can provide a solution to the current global warming problem.[4] One of the envisaged products is methane. It presents several advantages over other chemicals because it can be directly injected into already existing natural gas pipelines, and it can be used as a fuel or raw material for the production of chemicals. The methanation of CO_2, also known as the Sabatier reaction (eq 1), is an exothermic reaction that can be used for this purpose, provided that H_2 is obtained from renewable sources.

$$CO_2 + 4H_2 \rightarrow CH_4 + 2H_2O \qquad \Delta H^0 = -165\ kJ/mol \tag{1}$$

The major challenges for an industrial implementation of this reaction are to increase the activity and selectivity to methane that can permit the operation at low temperature and pressures in compact units that should be close to CO_2 emission sources.

The more active and selective materials for this reaction are supported Ru and Rh-based catalysts.[5−9] Ru/TiO_2[10] and Rh/γ-Al_2O_3[11] catalysts can be active at near room temperatures with 100% methane selectivity. In the case of supported Rh, recent works studied the effect of support and metal particle size in the rate of reaction, showing that larger particles (>7 nm) are more active as a result of a lower coverage of CO(ads)

Received: July 18, 2013
Revised: September 17, 2013
Published: October 9, 2013

   dx.doi.org/10.1021/cs400576w | ACS Catal. 2013, 3, 2799−2812

intermediates.[12] Rh carbonyl hydride has been shown to be a key intermediate over Rh/γ-Al_2O_3 catalysts.[6,13] Pd catalysts have also been shown to be active in CO_2 methanation, but only at temperatures higher than 300 °C, presenting lower selectivity to CH_4 than Rh-based catalysts because Pd is a good water-gas shift catalyst, thus producing CO in significant amounts.[9,14] Pd/SiO_2's modified by Mg, Fe, or Ni were tested in CO_2 methanation at high temperatures (450 °C), which always gave a significant amount of undesired CO.[15] Catalysts containing Rh and Pd have also been studied in other gas phase heterogeneous catalytic reactions, such as CO oxidation,[16] hydrogen production from ethanol,[17] methane decomposition,[18] and methane combustion,[19] showing that the association of the two metals leads to higher catalytic performances.

In the case of CO_2 methanation, Rh−Pd bimetallic catalysts have not been studied so far. The potentialities of such bimetallic catalysts seem to be important, especially when looking at recent results on other bimetallic systems in this reaction: Ni−Fe/Al_2O_3 catalysts showed a higher activity compared to pure Ni/Al_2O_3, although no mechanistic explanations were given.[20] The effect of the presence of two metals in the catalyst was recently studied by Swalus et al.[21] They mixed a Rh/γ-Al_2O_3 catalyst with Ni supported on active carbon (Ni/C), a material known to store H_2 in significant amounts. Methanation experiments at 125 °C and 3 bar were performed by sending a pulse of CO_2 to a flow of H_2 passing through a Rh/γ-Al_2O_3 + Ni/C catalyst. Methane production rates increased per mole of Rh in the catalyst when Ni/C catalyst was present. The authors invoked a cooperation effect between the two catalysts, in which hydrogen is activated on Ni/C and transferred to Rh/γ-Al_2O_3, where it reacts with CO(ads) species, and thus, the rate of reaction is increased. The rate-determining step in CO_2 methanation has been proposed to be the dissociation of CO adsorbed species.[8,12,22−24] To get more insight into the mechanistic aspects controlling the cooperation between metallic phases in CO_2 methanation, we studied the interaction between a catalyst that is inert in the hydrogenation of CO_2 at low temperature (Pd/γ-Al_2O_3) and a known active catalyst, such as Rh/γ-Al_2O_3.

The strategy followed in this work was to study catalysts composed of mechanical mixtures with different proportions of Rh/γ-Al_2O_3 and Pd/γ-Al_2O_3 catalysts. We have adopted this procedure because by simple mixing of already prepared catalysts, there is less probability of the formation of bimetallic structures during the reaction, and thus, the role and the functions of the different catalysts during the reaction are more clearly studied and put in evidence. The two metals were supported on the same support to focus on the effect of metallic phases rather than on the support. The in situ DRIFTS technique was used to assess the synergistic effects by studying the nature and reactivity of surface species on bimetallic catalysts compared with monometallic ones. Kinetic experiments, on the other hand, permitted obtaining useful information about the coverage and adsorption strength of surface intermediates. The oxidation state and surface concentration of the metals were investigated by XPS.

2. EXPERIMENTAL SECTION

2.1. Preparation of Catalysts. *2.1.1. Monometallic Catalysts.* Rh(2 wt %)/γ-Al_2O_3 catalyst was prepared by wet impregnation. $RhCl_3$*xH_2O (Alfa Aesar, CAS 20765-98-4) was used as the metallic precursor, and the support was γ-Al_2O_3 (Alfa Aesar, CAS 1344-28-1, 99.97%). Eight grams of support was suspended in 400 mL of distilled water; 0.3868 g of Rh precursor was added to obtain a catalyst with 2 wt % of metallic Rh. After stirring for 4 h and evaporating the solvent under reduced pressure in a rotavapor at 40 °C, the sample was dried at 110 °C overnight and then calcined in a static-air oven at 450 °C for 4 h (heating ramp 10 °C/min). Reduced Pd (5 wt %)/γ-Al_2O_3 catalyst was purchased from Alfa Aesar (ref: 11713).

2.1.2. Mechanical Mixtures. Mechanical mixtures with different proportions of Rh(2 wt %)/γ-Al_2O_3 and Pd(5 wt %)/γ-Al_2O_3 catalysts were prepared by adding the required mass of the catalysts to *n*-pentane (Sigma-Aldrich, Purity >99%) at a ratio of 1 g of catalyst per 100 mL of *n*-pentane, followed by stirring for 1 h at room temperature. The liquid was gently evaporated at 30 °C overnight. Catalysts are labeled Rh*X*-Pd*Y*, where *X* and *Y* correspond to the mass percentage of Rh(2 wt %)/γ-Al_2O_3 and Pd(5 wt %)/γ-Al_2O_3 in the sample, respectively. Pd100 and Rh100 correspond to pure Pd(5 wt %)/γ-Al_2O_3 and Rh(2 wt %)/γ-Al_2O_3 catalysts, respectively. The resulting mechanical mixtures were pressed, ground, and sieved to obtain a significant amount of the 100−315 μm particle fraction, which was afterward used in catalytic tests. Mixtures were not calcined after preparation.

2.2. Characterization of Catalysts. *2.2.1. Nitrogen Physisorption.* N_2 adsorption and desorption isotherms were obtained at −196 °C using a Micromeritics Tristar 3000 instrument. Samples were degassed at 0.15 mbar and 150 °C overnight prior to analysis. The BET isotherm and BJH model were used to obtain specific surface area and pore volume, respectively.

2.2.2. H_2 Chemisorption. H_2 chemisorption at 35 °C was used to measure the amount of exposed metal atoms. Experiments were performed with an ASAP 2010C apparatus from Micromeritics. About 0.15 g of catalyst was loaded into a Pyrex tube and subsequently heated in He (Praxair 5.0, 20 mL/min) at 120 °C for 1 h. After evacuation, the sample was reduced at 350 °C during 1 h in pure H_2 (Praxair 5.0, 30 mL/min), followed by purging with He at the same temperature for 1 h and cooling in He to adsorption temperature. Two isotherms were measured in the range 0.08−95 kPa. The first accounts for reversible and irreversible chemisorption. The sample was evacuated to desorb irreversibly adsorbed hydrogen. The second isotherm was then measured, which accounts only for the reversibly adsorbed hydrogen. The subtraction of the linear part of the two isotherms gave the total amount of irreversibly adsorbed (chemisorbed) hydrogen. The amount of surface metal atoms was calculated assuming a chemisorption stoichiometry for rhodium of H/Rh = 1[25] and for palladium, H/Pd = 1.[26] Dispersion was defined as the amount of metal atoms on the surface divided by the total metal atoms in the catalyst.

2.2.3. X-ray Photoelectron Spectroscopy. XPS analyses were performed with a SSI-X-probe (SSX-100/206) photoelectron spectrometer equipped with a monochromatic microfocused Al Kα X-ray source (1486.6 eV) from Surface Science Instruments. The sample powders were pressed into small stainless steel troughs mounted on a multispecimen holder. The samples were outgased overnight under vacuum (10^{-5} Pa) and then introduced into the analysis chamber, where the pressure was around 10^{-7} Pa. Fresh catalysts (i.e., after *n*-pentane stirring and drying) as well as spent catalysts were analyzed. Spent catalysts were retired from the reactor and stored. They were finely ground before pressing them in the troughs.

An electron flood gun set at 8 eV and a Ni grid placed at 3 mm above the sample were used to standardize charging effects. Pass energy of the analyzer was 150 eV, and the spot size was ~1.4 mm^2. The atomic concentration ratios were calculated by normalizing surface area ratios with sensitivity factors based on Scofield cross sections. In addition, all binding energies were calculated, taking as reference the C−(C, H) component of the C 1s adventitious carbon peak fixed at 284.8 eV. Peak decomposition was performed using the CasaXPS program (Casa Software Ltd., UK) with a Gaussian/Lorentzian (85/15) product function and a Shirley nonlinear sigmoid-type baseline. The following peaks were used for the quantitative analysis: O 1s, C 1s, Al 2p, Rh 3d, and Pd 3d.

2.3. In Situ DRIFTS. In situ diffuse reflectance Fourier transform infrared spectroscopy (in situ DRIFTS) spectra were collected on a Bruker Equinox 55 infrared spectrometer equipped with an air cooled MIR source with KBr optics and a MCT detector. Spectra were obtained by collecting 200 scans with a resolution of 4 cm^{-1} and are presented in absorbance units. It has been shown that absorbance can be used to estimate the surface concentration of adsorbate, provided that the relative reflectance is higher than 60%.[27] This condition was fulfilled in our study.

A background was recorded before starting the experiment by placing an aluminum mirror in the sample holder. In that way, the signals due to impurities in the cell windows or gases inside the spectrometer were subtracted. Samples were placed without packing or dilution inside a cell with controlled temperature and environment reflectance (Spectra-Tech 0030-103) equipped with ZnSe windows. Different mixtures of gases could be sent to the cell (He (Praxair 4.8), H_2 (Praxair 3.5), CO_2 (Praxair 4.8)), and their flow rates were controlled by high precision gas rotameters. The gases at the outlet of the cell were analyzed by a quadrupole mass spectrometer (Balzers QMS 200) by following the evolution of the m/z = 2 (H_2), 15 (CH_4), 18 (H_2O), 28 (CO), and 44 (CO_2). The response time of the mass spectrometer following a change in gas concentration was <60 s.

Catalysts recovered after standard catalytic tests in fixed bed reactor were finely ground and loaded onto the sample holder. Once the catalyst was placed in the cell, it was flushed with He (20 mL/min) for 10 min and then reduced in a flow (20 mL/min) of a reductive mixture consisting of H_2 (5 vol %) diluted in He (95 vol %) during 1 h at 300 °C. Since spent catalysts were used and these were already reduced, a mild reduction procedure was applied here to standardize the procedure for all the catalysts. After reduction, the cell was cooled to 50 °C in the same gas mixture. Reaction was carried out sending to the cell 20 mL/min of a mixture composed of CO_2 (10 vol %) and H_2 (40 vol %) diluted in He. The sample was kept at 50 °C for 20 min, which was sufficient to ensure steady state activity and constant spectra. Two types of experiments could be done starting from this point:

(a) Steady state experiments: The system was then stepwise heated (5 °C/min) to 100, 150, and 200 °C maintaining the sample 20 min at each temperature.
(b) Transient experiments: The catalyst was heated under reactive mixture at 5 °C/min to the desired temperature (150, 175, or 200 °C), and after 20 min at that temperature, the flow was changed to H_2 (8 mL/min) diluted in He (10 mL/min). Spectra were recorded every 5 min.

Decomposition of the CO adsorbed spectral region was performed using the CasaXPS program, which has been already used for treating DRIFTS data.[28] A Gaussian/Lorentzian (70/30) product function was used with a linear baseline (from 1700 to 2100 cm^{-1}). The position of the peaks was fixed taking into account the data acquired for pure Pd100 and Rh100 catalysts. Those positions were subsequently used to fit the peaks of the mechanical mixtures. The positions of the peaks were allowed to vary ±10 cm^{-1} for bridge-bonded CO peaks and ±3 cm^{-1} for linearly adsorbed CO peaks. The full width at half-maximum (fwhm) values were not fixed but allowed to vary freely as long as acceptable fits were obtained.

2.4. Catalytic Activity Measurements. Standard catalytic tests were carried out using a quartz reactor (U-shaped) with 0.4 cm i.d. A section in the center of the tube is expanded with a diameter of 1 cm, in which the catalyst (200 mg, 100−315 μm particle size) was placed and supported by a quartz frit. A thermocouple was in contact with the central part of the catalyst bed and was used to measure and control the temperature. Heat and mass transfer effects were ruled out using criteria presented elsewhere.[29] Thus, it can be safely assumed that the reaction took place in a fully kinetic regime.

The reaction was carried out at atmospheric pressure by reducing the catalyst in a 30 mL/min flow of pure H_2 (Praxair 3.5) for 1 h (ramp 10 °C/min) at 350 °C. Afterward, the reactor was cooled to 50 °C, and the reaction mixture (20 mL/min) was admitted (CO_2 (Praxair 4.8, 10 vol %), H_2 (40 vol %) diluted in He (Praxair 4.8)). Measurements were performed at various temperatures between 50 and 200 °C (with 1 h at each temperature to ensure steady state conditions). Exit gases were quantified using a gas chromatograph (Varian CP3800) equipped with Hayesep Q, Molsieve 5A, and CP-Sil-5CB columns. The separated gases were detected with a flame ionization detector (CH_4) and a thermal conductivity detector (CO and CO_2). All transfer lines were maintained at 120 °C to avoid water condensation.

Reaction rates were determined at CO_2 conversions lower than 10% to ensure differential reactor conditions. The mass-specific reaction rate was defined as the number of moles of CH_4 produced per total mass of catalyst per second. A Rh-specific reaction rate was defined as the number of moles of CH_4 produced per mole of Rh loaded to the catalyst per second. The intrinsic reaction rate (turnover frequency, TOF), was defined as the number of molecules of CH_4 produced per metal surface atom (Rh and Pd) per second. The number of metal surface atoms was obtained from dispersion data.

Apparent reaction orders with respect to H_2 and CO_2 were determined in a series of tests in which the partial pressure of one reactant was kept constant, whereas the partial pressure of the other was varied, at constant temperature. The concentration of He was varied accordingly in order to keep the total flow at 20 mL/min. In such tests, the space velocity was changed by varying the mass of catalyst to compare kinetic parameters at similar CO_2 conversions. The reaction orders were calculated by fitting the following power law rate equation,

$$r = A e^{-E_{app}/RT} P_{CO_2}^{a} P_{H_2}^{b} \quad (2)$$

where r is the methane formation rate; A is the apparent pre-exponential factor; E_{app} corresponds to the apparent activation energy; and a and b are CO_2 and H_2, the apparent reaction orders, respectively.

dx.doi.org/10.1021/cs400576w | ACS Catal. 2013, 3, 2799−2812

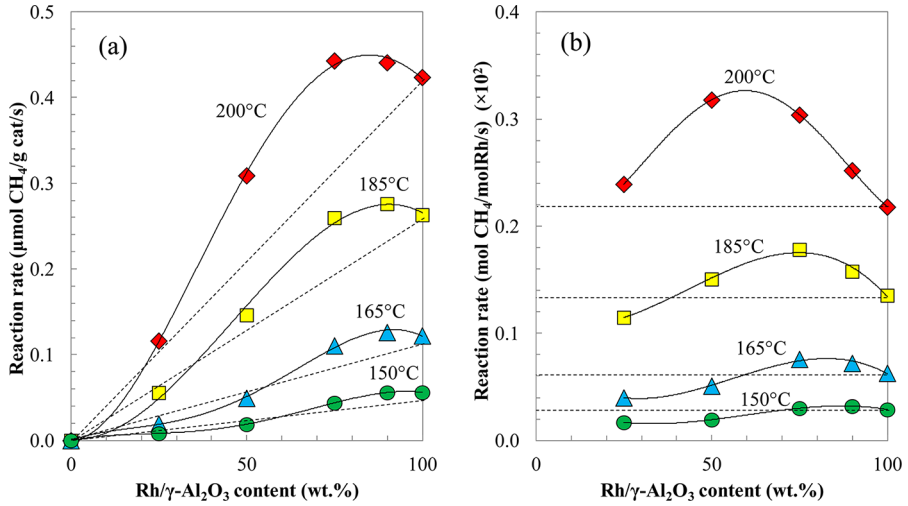

Figure 1. (a) Specific reaction rate as a function of the content of Rh (2 wt %)/γ-Al_2O_3 in the mechanical mixtures. Dotted lines represent the linear interpolation between the activity of pure Rh (2 wt %)/γ-Al_2O_3 and pure Pd (5 wt %)/γ-Al_2O_3. (b) Specific reaction rate expressed per mole of Rh in the catalyst, as a function of Rh (2 wt %)/γ-Al_2O_3 content in the mechanical mixture. Horizontal dotted lines are shown to compare with the activity of pure Rh (2 wt %)/γ-Al_2O_3 catalyst.

Table 1. Reaction Parameters at 200°C[a]

	CO_2 conversion (%)	CH_4 rate (μmol g_{cat}^{-1} s^{-1})	CH_4 rate ($\times 10^2$ mol mol_{Rh}^{-1} s^{-1})	CH_4 TOF[b] ($\times 10^2$ s^{-1})	E_a[c] (kcal/mol)	apparent reaction order	
						H_2[d]	CO_2[d]
Rh100	6.2	0.424	0.218	1.002	16.4	0.55	0.23
Rh90−Pd10	6.4	0.441	0.252	0.963	17.2	n.d.	n.d.
Rh75−Pd25	6.5	0.443	0.304	0.869	19.3	0.53	0.12
Rh50−Pd50	4.5	0.309	0.318	0.443	21.6	n.d.	n.d.
Rh25−Pd75	1.7	0.116	0.239	0.170	21.1	0.57	−0.03
Pd100	0 (4.3[e])	0 (0.187[e])		0 (0.242[e])	23.5[f]	0.81[e]	−0.09[e]

[a]CO_2 conversion, specific reaction rates, turnover frequency for methane formation, apparent activation energy, and apparent reaction orders; n.d., not determined. [b]Turnover frequency calculated taking into account the amount of surface metal (both Pd and Rh). For mechanical mixtures, total surface metal was obtained by interpolation from the two pure catalysts. [c]Activation energy calculated from kinetic data obtained between 150 and 200 °C. [d]Data obtained at 200 °C. [e]Data obtained at 300 °C. [f]Activation energy calculated from kinetic data obtained between 250 and 350 °C.

3. RESULTS

3.1. Catalytic Activity. Figure 1a shows the catalytic activity of the different mechanical mixtures in CO_2 methanation at different temperatures. The only carbon-containing product detected was CH_4; the selectivity, thus, was 100% in all the experiments. Pd100 catalyst was not active under these experimental conditions. The dotted line shows the theoretical activity calculated by simple interpolation of the activity of Rh100 and Pd100 catalysts. The activity of mixed catalysts lies well above these curves, especially at higher temperatures, showing that the mechanical mixture of the two catalysts has a positive effect in the rate of methane formation. It is observed that the synergy is higher for Rh75−Pd25 and Rh90−Pd10 catalysts, whereas when the amount of Rh/γ-Al_2O_3 catalyst in the mixture is too small, the synergy is not observed. When the rate of reaction is expressed in terms of total Rh content in the mechanical mixtures (Figure 1b), it can be clearly seen that the reaction rate is significantly increased compared with the pure Rh100 catalyst. We recall that Pd100 catalyst is fully inactive under these conditions. At 200 °C, the rate of the Rh50−Pd50 mixture is 50% higher than the Rh100 catalyst, comparing using Rh content. The maximum is located between Rh50−Pd50 and Rh75−Pd25 catalysts. When the content of Rh/γ-Al_2O_3 is higher, as in the case of the Rh90−Pd10 sample, the activity per Rh atom decreases and approaches that of the Rh100 catalyst. When the amount of Rh/γ-Al_2O_3 is lower than 50%, the activity decreases and can even attain values that are lower than for the pure Rh/γ-Al_2O_3 catalyst. This effect is more marked at lower temperatures.

Table 1 shows the conversion of CO_2 and specific rate of methane formation as a function of the composition of the mechanical mixtures. It is observed that higher conversions are obtained for samples containing 75 wt % of Rh/Al_2O_3. When rates are normalized by the amount of surface metal (Rh and Pd) in the catalysts, which was obtained from H_2 chemisorption data (Table 2), the maximum rate is observed for Rh100 sample. When the amount of Rh/γ-Al_2O_3 is decreased, the

Table 2. BET Surface Area and H_2 Chemisorption Results

	BET surface area (m^2/g)	pore vol (cm^3/g)	surface metal (μmol/g)	metal dispersion
Rh100	71.4	0.37	42.3	0.22
Rh50−Pd50[a]			69.8 (59.8[b])	0.21 (0.19[b])
Pd100	140	0.62	77.2	0.16

[a]For this catalyst, the amount of surface metal and dispersion comprise both Pd and Rh. [b]Interpolated from the pure catalysts.

dx.doi.org/10.1021/cs400576w | ACS Catal. 2013, 3, 2799−2812

turnover frequency also decreases. Pd100 catalyst was not active at 200 °C. At 300 °C, Pd100 showed activity toward methane and CO formation, with 60% methane selectivity. At 300 °C, Pd100 catalyst presented a TOF of 0.242×10^{-2} s^{-1}, which is still lower than that observed at 200 °C for the majority of Pd/γ-Al_2O_3–Rh/γ-Al_2O_3 mixtures. The apparent activation energies of methane formation for the mechanical mixtures and pure catalysts are shown in Table 1. When the proportion of Pd/γ-Al_2O_3 catalyst in the mixture increases, the apparent activation energy also increases, from 16.4 to 21–22 kcal/mol, approaching that of the Pd100 sample (23.5 kcal/mol).

Figure 2a shows the methane formation rate as a function of CO_2 partial pressure at 200 °C. Rh100 catalyst shows an apparent CO_2 order of 0.23. In the case of Rh75–Pd25 catalyst, the CO_2 reaction order decreases to 0.12. Further increase in Pd/γ-Al_2O_3 loading results in a decrease of CO_2 reaction order,

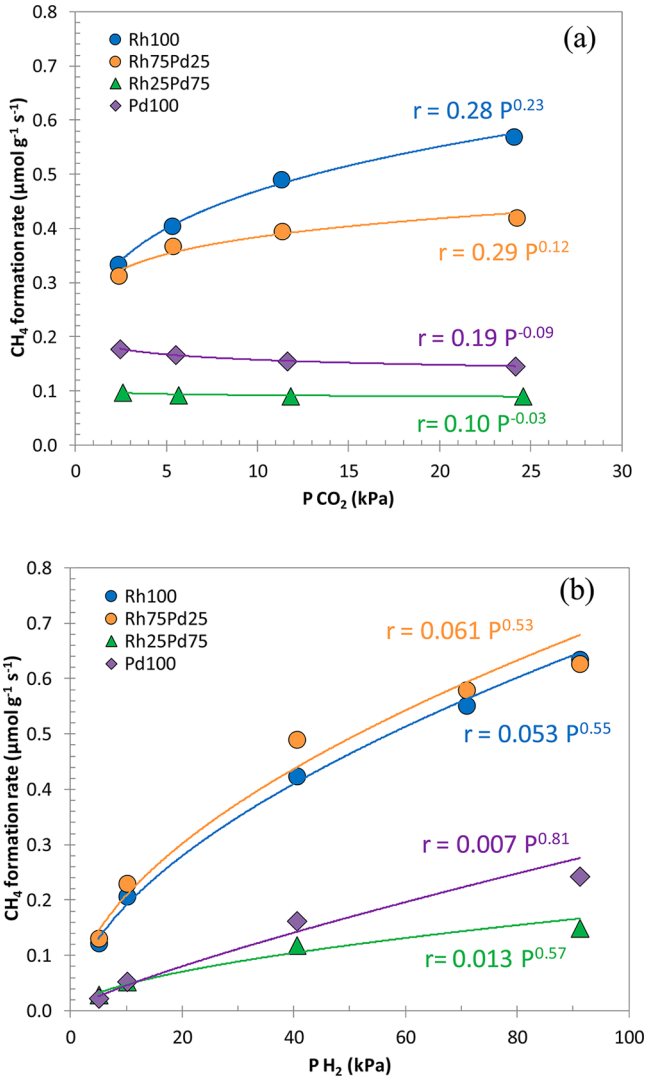

Figure 2. Apparent CO_2 and H_2 reaction orders at 200 °C (excepting Pd100, whose activity data were collected at 300 °C). (a) Rate dependence on CO_2 partial pressure at constant H_2 partial pressure (40.5 kPa). (b) Rate dependence on H_2 partial pressure at constant CO_2 partial pressure (10.1 kPa). In both cases, the concentration of He was varied to maintain a total pressure of 101.3 kPa and a total flow rate of 20 mL/min.

reaching a value of −0.09 for pure Pd/γ-Al_2O_3 (at 300 °C). The same procedure was applied to study the effect of H_2 partial pressure, and the results are plotted in Figure 2b. H_2 has a more beneficial effect in reaction rates than CO_2 because the orders are positive for all the catalysts. Catalysts containing Rh/γ-Al_2O_3 present H_2 apparent reaction orders between 0.53 and 0.57. There are no significant variations in H_2 reaction order when the content of Pd/γ-Al_2O_3 in the mixture is varied. In the case of pure Pd/γ-Al_2O_3, the H_2 apparent reaction order is 0.81, which is higher than that of Rh/γ-Al_2O_3-containing samples.

3.2. Catalyst Characterization. Figure 3 shows the H_2 adsorption isotherms of Rh100, Pd100, and Rh50–Pd50 catalysts. The isotherm for Rh100 (Figure 3a) shows the typical shape of the adsorption isotherm of hydrogen on the metal-supported catalysts. In the case of the Pd100 sample (Figure 3b), there is a steep increase in the amount of adsorbed H_2 when the pressure is raised above 3 kPa. This has been ascribed to the formation of β-hydride in Pd particles.[30] In the case of the Rh50–Pd50 catalyst (Figure 3c), the β-hydride formation on Pd is also observed, as well as the slow increase in the amount adsorbed with pressure that was observed in the case of pure Rh100 catalyst.

Table 2 shows that the dispersion of pure Rh/γ-Al_2O_3 is 0.22, and for Pd/γ-Al_2O_3 catalyst, is 0.16. Rh50–Pd50 catalyst presents a dispersion of 0.21, which agrees well with the theoretical value calculated by interpolation using the dispersions of monometallic catalysts (0.19). Consequently, one can safely assume that for the other mixed catalysts, the calculated dispersion values should be similar to the experimental ones. The amount of surface metal (Pd and Rh) was obtained taking into account the dispersion and the actual metal loading. Surface metal atoms ranged from 42.3 μmol/g in the case of Rh100 and 77.2 μmol/g for Pd100 catalyst. The surface area of the catalysts was 71.4 m^2/g for Rh100 and 140 m^2/g for Pd100. The solids contain meso and macropores.

Table 3 shows the position of the XPS peaks of $Pd3d_{5/2}$ and $Rh3d_{5/2}$ electrons for fresh catalysts. In the case of Pd, the recorded binding energy was 334.8 eV for pure Pd/γ-Al_2O_3 catalyst. For mixtures with Rh/γ-Al_2O_3 addition, the binding energy did not change appreciably, ranging from 334.9 to 335.1 eV. Such values are characteristic of metallic palladium (Pd^0).[31,32] In the case of Rh90–Pd10 catalyst, the XPS signal for $Pd3d_{5/2}$ was too weak to obtain a precise value of binding energy. Pure Rh/γ-Al_2O_3 catalyst shows a $Rh3d_{5/2}$ binding energy of 309.7 eV. Mechanical mixtures show similar $Rh3d_{5/2}$ binding energies (309.6–309.7 eV). These binding energies are characteristic of the presence of Rh^{3+} from supported Rh_2O_3 species.[6,33]

XPS binding energies for catalysts recovered after reduction pretreatment and catalytic test are shown in Table 4. In the case of $Pd3d_{5/2}$ binding energies, the catalysts present similar binding energies than in the case of fresh catalysts, with values ranging from 334.7 eV for Pd100 and 335.1 eV for Rh75–Pd25. The full width at half-maximum (fwhm) of $Pd3d_{5/2}$ also presents similar values, between 2.72 and 3.24 eV. The spectrum of $Rh3d_{5/2}$ electrons for spent catalysts was decomposed in two peaks: one at low binding energy centered at 307.3 eV and other at higher binding energy at 308.9–309.0 eV. $Rh3d_{5/2}$ electrons with binding energy of 307–307.3 eV have been usually assigned to metallic Rh species (Rh^0).[33,34] The component appearing at 308.9–309.0 eV can be associated with Rh^{3+} species. The proportion of reduced (Rh^0) and oxidized (Rh^{3+}) species after reaction is similar for all the

dx.doi.org/10.1021/cs400576w | ACS Catal. 2013, 3, 2799–2812

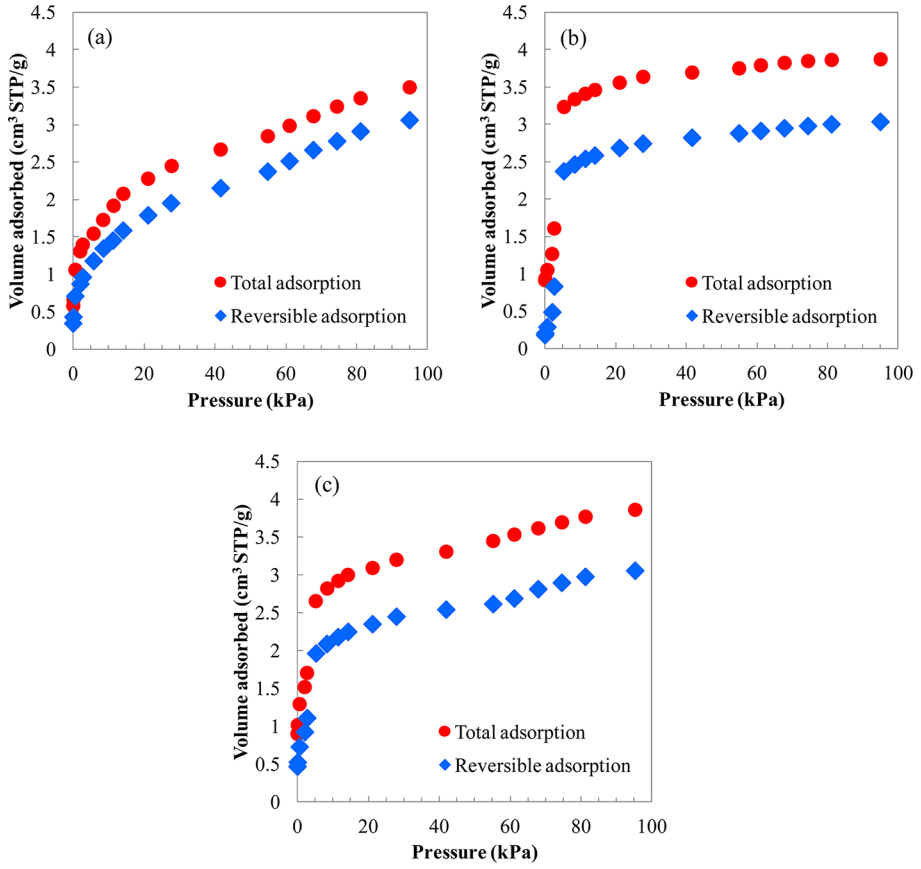

Figure 3. Hydrogen chemisorption isotherms at 35 °C for (a) Rh100, (b) Pd100, and (c) Rh50−Pd50 catalysts.

Table 3. XPS Results for Fresh Catalysts[a]

	Pd $3d_{5/2}$		Rh $3d_{5/2}$	
catalyst	position (eV)	fwhm (eV)	position (eV)	fwhm (eV)
Pd 100	334.8	2.76		
Rh25−Pd75	334.9	2.84	309.5	3.02
Rh50−Pd50	335.1	2.93	309.5	3.01
Rh75−Pd25	335.1	3.24	309.6	2.92
Rh90−Pd10	n.m.	n.m.	309.6	2.86
Rh100			309.7	2.72

[a]Position and full width at half maximum (fwhm) of Pd $3d_{5/2}$ and Rh $3d_{5/2}$ species.

samples containing Rh, ranging about 50% for each species. It is worth noting that the binding energies of other elements, such as Al 2p (74.4−74.5 eV) and O 1s (531.2−531.3 eV) did not show significant variations among the catalysts either before or after reaction, and thus, they are not shown. The presence of Cl species coming from the $RhCl_3$ precursor used for Rh/γ-Al_2O_3 preparation was not detected by XPS on any sample, before or after reaction.

The concentration of Rh and Pd on the surface expressed as XPS atomic ratios are presented in Table 5. The Rh/Al atomic ratios for all Rh-containing catalysts show a decrease after reduction treatment and reaction. The same occurs for Pd/Al atomic ratios in the case of Pd-containing samples. To compare the evolution of Pd and Rh surface concentrations between fresh and spent catalysts, the atomic ratio Rh/(Pd + Rh) was calculated. The Rh/(Pd + Rh) XPS atomic ratio is higher for catalysts that are rich in Rh. When comparing between fresh and used samples, it is observed that the Rh/(Pd + Rh) XPS atomic ratio does not change appreciably for any catalyst.

3.3. In Situ DRIFTS. *3.3.1. Steady State Conditions.* Figure 4 shows the evolution in temperature of DRIFT spectra

Table 4. XPS Results for Spent Catalysts[a]

	Pd $3d_{5/2}$			Rh $3d_{5/2}$, HBE			Rh $3d_{5/2}$, LBE		
catalyst	position (eV)	fwhm (eV)	%	position (eV)	fwhm (eV)	%	position (eV)	fwhm (eV)	%
Pd 100	334.7	2.78	100						
Rh25−Pd75	334.8	2.72	100	308.9	3.40	54	307.3	2.54	46
Rh50−Pd50	334.9	2.93	100	309.0	3.48	47	307.3	2.43	53
Rh75−Pd25	335.1	3.24	100	308.9	3.51	50	307.3	2.37	50
Rh90−Pd10	n.m.	n.m.	100	309.0	3.28	51	307.3	2.36	49
Rh100				309.0	3.50	44	307.3	2.52	56

[a]Position, full width at half maximum (fwhm) and relative concentration. Pd $3d_{5/2}$ peak and high binding energy (HBE) and low binding energy (LBE) components of Rh $3d_{5/2}$ peak; n.m, not measurable.

dx.doi.org/10.1021/cs400576w | ACS Catal. 2013, 3, 2799−2812

Table 5. XPS Results[a]

	Rh/Al		Pd/Al		Rh/(Pd+Rh)	
	fresh	spent	fresh	spent	fresh	spent
Rh100	0.0257	0.0194			1.00	1.00
Rh90−Pd10	0.0238	0.0179	0.0020	0.0016	0.92	0.92
Rh75−Pd25	0.0210	0.0182	0.0036	0.0035	0.85	0.84
Rh50−Pd50	0.0186	0.0147	0.0082	0.0066	0.70	0.69
Rh25−Pd75	0.0107	0.0090	0.0144	0.0111	0.43	0.45
Pd100			0.0222	0.0181	0.00	0.00

[a]Surface concentrations expressed as Rh/Al, Pd/Al and Rh/(Pd+Rh) atomic ratios for fresh and spent catalysts.

obtained for representative catalysts in CO_2 methanation at steady state conditions. All the significant spectral changes are contained in the wavenumber region between 1200 and 2200 cm^{-1}. The region in which OH groups appear (3000−3800 cm^{-1}) does not show significant changes. Moreover, the vibrations of CH_x species that appear at 2800−3000 cm^{-1} were very weak and did not show significant variations that permit obtaining valuable information from them; hence, they are not shown. Figure 4a shows the evolution of the surface species of Rh100 catalyst. At 50 °C, a strong and broad peak appears at 2046 cm^{-1} that is characteristic of Rh−CO species adsorbed in linear form.[24,35−37] A very strong peak that appears at 1630 cm^{-1} is usually ascribed to the presence of adsorbed water on the support.[38]

A further increase in the temperature to 100 °C leads to an increase in the intensity of the linear Rh−CO peak. There is also the apparition of peaks at 1374 and 1589 cm^{-1} that are associated with O−C−O stretching vibrations of adsorbed formate ion[36,39] or carbonates,[40,41] both adsorbed on Al_2O_3. The band at 1393 cm^{-1} arises from the C−H deformation mode of surface formate.[39] A broad and weak band appears around 1800 cm^{-1}. This band is assigned to CO adsorbed in bridged form on Rh (Rh_2−CO).[42−44] Further increments in temperature lead to an increase in the intensity of the Rh−CO linear band, and at the same time, the band shows a shift to lower wavenumbers, reaching 2023 cm^{-1}.

In the case of the Pd100 catalyst (Figure 4c), at 50 and 100 °C, no peaks coming from adsorbed CO species on Pd are detected. The main peaks at this stage are those coming from formate or carbonate species adsorbed on the support (1374, 1393, and 1590 cm^{-1}). When the temperature is raised to 150 °C or above, a broad band develops at 1880 cm^{-1} and then shifts to 1900 cm^{-1} with a concomitant increment in its intensity. This band is ascribed to bridge-bonded CO adsorbed on Pd (Pd_2−CO).[45] A very weak band appears at 2038 cm^{-1}, which can be associated with Pd−CO in linear form.[45] Bands other than adsorbed CO are the same as in the case of pure Rh100 catalyst, with the exception of a band appearing at 1465 cm^{-1} that in the case of Rh100 is hardly visible. This peak is assigned to carbonate species.[39,41]

Figure 4b shows the spectra at steady state of Rh50−Pd50 mechanical mixture as a function of temperature. At 50 °C, the peak characteristic of Rh−CO in linear form appears here at lower wavenumbers (2036 cm^{-1}). A further increase in the temperature produces an augmentation of the intensity of the linear Rh−CO band, which here show two peaks, one at 2042 and the other at 2023 cm^{-1}. When the temperature is increased, the peak at 2023 cm^{-1} becomes more intense compared with that appearing at 2042 cm^{-1}. The interval of wavenumbers in which bridge-bonded adsorbed CO species appear (1800−1900 cm^{-1}) shows a very broad peak, indicating that both Rh−CO and Pd−CO bridged species coexist. The region from 1200 to 1700 cm^{-1} shows the same carbonate and formate bands that were detected in the case of pure catalysts.

To provide a quantification of the adsorbed CO species, a decomposition of the peaks was performed. In Figure 5 are shown the decomposed spectra for each catalyst at 200 °C and steady state CO_2 methanation conditions. In the case of the Pd100 catalyst, the only resolved peak corresponds to bridged Pd−CO species, appearing at 1890−1900 cm^{-1}. For the pure Rh100 catalyst, three peaks were needed to resolve the spectra. The first corresponds to bridged Rh−CO species, which appears at 1800−1810 cm^{-1}. The other two were needed to fit the asymmetric peak of linear Rh−CO species. The main peak was fixed at 2027−2030 cm^{-1}, and the "tail" to lower wavenumbers was fitted with a peak centered at 1987−1990 cm^{-1}. In the case of catalysts containing both metals, the same features are observed, in addition to another peak at 2048−

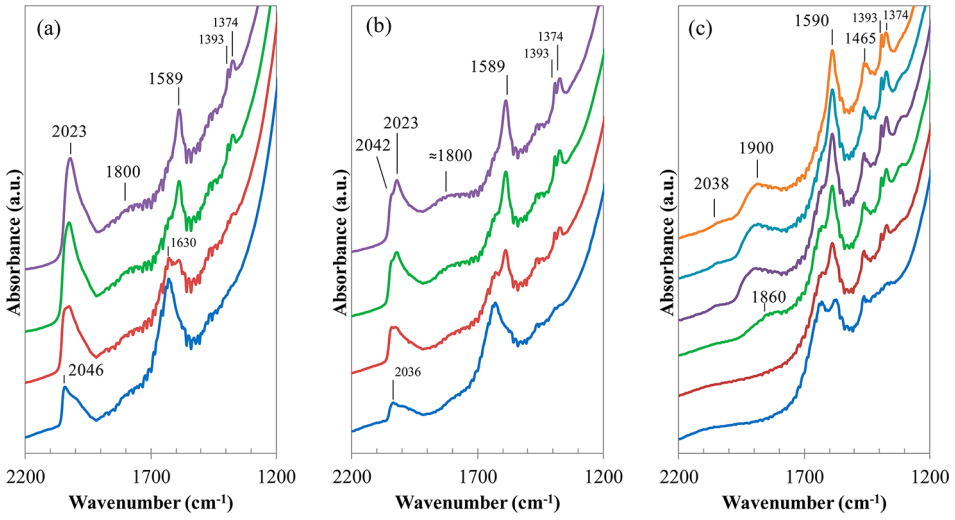

Figure 4. DRIFT spectra as a function of temperature at steady state CO_2 methanation conditions: (a) Rh100, (b) Rh50−Pd50, (c) Pd100. From bottom to top: 50, 100, 150, 200 °C. In the case of Pd100, from bottom to top: 50, 100, 150, 200, 250, and 300 °C.

dx.doi.org/10.1021/cs400576w | ACS Catal. 2013, 3, 2799−2812

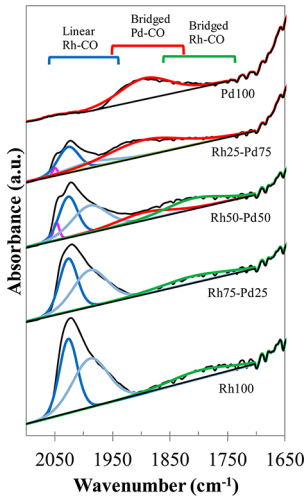

Figure 5. DRIFTS spectra of all the catalysts in CO_2 methanation at steady state at 200 °C. Decomposition peaks are indicated.

2051 cm^{-1} that accounts for the shoulder observed in the Rh−CO linear peak of Rh50−Pd50 and Rh25−Pd75 catalysts.

The areas of the three linear Rh−CO bands were added for each catalyst. The total area was then normalized using the Rh loading of the catalyst. The results are shown in Figure 6 for

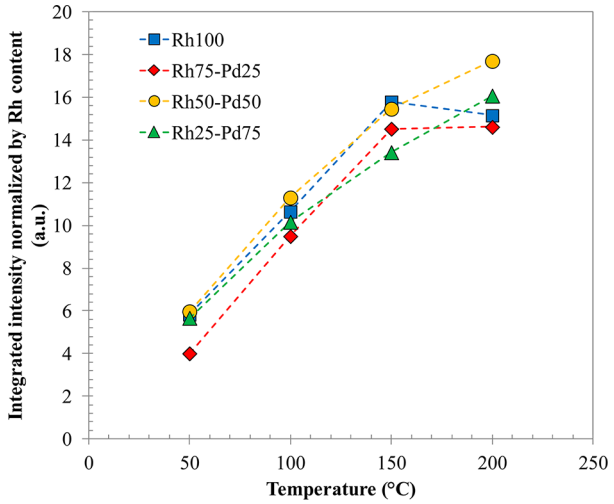

Figure 6. DRIFTS results. Integrated intensity of the summation of linear Rh−CO peaks as a function of temperature in CO_2 methanation at steady state. Peak areas were normalized using Rh loading.

steady state CO_2 methanation conditions as a function of temperature. The area of the linear Rh−CO peak increases as the temperature is raised and is similar for all Rh-containing samples up to 150 °C. When the temperature is increased to 200 °C, some differences arise among the catalysts. The Rh100 catalyst presents a slight decrease in the coverage of linear Rh−CO species, and Rh75−Pd25 shows stabilization in the amount of such species. In the case of Rh50−Pd50 and Rh25−Pd75 catalysts, the coverage of linear Rh−CO species continues to grow when the temperature is increased to 200 °C.

3.3.2. DRIFTS Transient Experiments. The reactivity of surface species was studied by means of transient experiments. The gas flow was changed from H_2 + CO_2 + He to H_2 + He by eliminating CO_2 from the mixture. In that way, we followed the reactivity of surface species as they react with hydrogen and are eliminated from the surface of the catalyst. Figure 7 shows the evolution of surface species upon a change in the flow from the standard reactive mixture to a CO_2-free flow at 175 °C. In the case of Rh100 catalyst (Figure 7a), the linear Rh−CO band decreases rapidly in intensity, and at the same time, it shifts to lower wavenumbers from 2025 to 2013 cm^{-1} after 40 min of exposure to H_2 + He flow. The peak associated with bridge-bonded Rh−CO species decreases more rapidly, disappearing completely after 10 min of exposure. Peaks associated with carbonates or formates appearing at wavenumbers lower than 1700 cm^{-1} do not show significant variations with time.

Figure 7b shows the results of the Rh50−Pd50 catalyst. In this case, the peaks associated with linear Rh−CO species decrease at a rate that is clearly lower than in the case of the Rh100 catalyst. In addition, the main peak appearing at 2023 cm^{-1} does not shift to lower wavenumbers after 40 min, as in the case of the Rh100 catalyst. The shoulder that appears at steady state at 2042 cm^{-1} progressively disappears. As in the case of the Rh100 catalyst, the band due to CO adsorbed in bridged form on Rh (1800 cm^{-1}) is very reactive and disappears completely after 20 min under hydrogen flow. The band associated with bridge-bonded Pd−CO (1900 cm^{-1}) also presents a rapid decrease, and no traces of it are observed after 20 min in H_2 flow. For pure Pd/γ-Al_2O_3 catalyst (Figure 7c), it is observed that the bridge-bonded Pd−CO peak, which appears at 1900 cm^{-1}, slowly disappears under H_2 flow at 175 °C. It presents a shift to 1880 cm^{-1} after 40 min on-stream. The peaks appearing at wavenumbers below 1700 cm^{-1} do not show significant variations, as in the case of the other catalysts.

Figure 8 shows the variation of the area (normalized by the area before gas switching) of bridged Pd−CO species during the transient experiment in CO_2-free mixtures. Bridged Pd−CO species of Pd100 catalyst decrease very slowly with time, and after 40 min, its concentration has decreased to 60%. In contrast, in the case of catalysts containing Rh (namely, the Rh25−Pd75 and Rh50−Pd50 catalysts), the reactivity of bridged Pd−CO species is considerably higher. The band disappeared completely after 25 min in the case of Rh25−Pd75 and after 20 min for Rh50−Pd50 catalyst.

Figure 9 shows the evolution of the area of linear Rh−CO species (considering the addition of the three peaks obtained in the decomposition, as it is shown in Figure 5) during the transient experiments in H_2 + He at 175 °C. Data shown were normalized by the area right before switching off the CO_2. The reactivity of linear Rh−CO species varies significantly among the catalysts. Rh100 shows the higher reactivity of linear Rh−CO species, followed by Rh75−Pd25 catalyst. Catalysts with lower Rh content show a very different behavior. The reactivity of linear Rh−CO species on these samples is much lower. Moreover, in the case of Rh25−Pd75, before 20 min on the H_2 + He stream, these species show a slow decrease to about 85% of their initial intensity. After that time, the band starts to decrease more rapidly, although at a rate that is still lower than in the case of the other catalysts.

4. DISCUSSION

4.1. Physicochemical Properties. Table 3 shows the binding energies of the main peak of both Rh and Pd for catalysts before te catalytic test. The binding energy of $Pd3d_{5/2}$ electrons indicates that metallic Pd is the main species on the surface of the Pd/γ-Al_2O_3 catalysts. There is a slight variation when the content of Pd/γ-Al_2O_3 decreases, from 334.8 to 335.1 eV. In the case of the catalysts recovered after the catalytic test

dx.doi.org/10.1021/cs400576w | ACS Catal. 2013, 3, 2799−2812

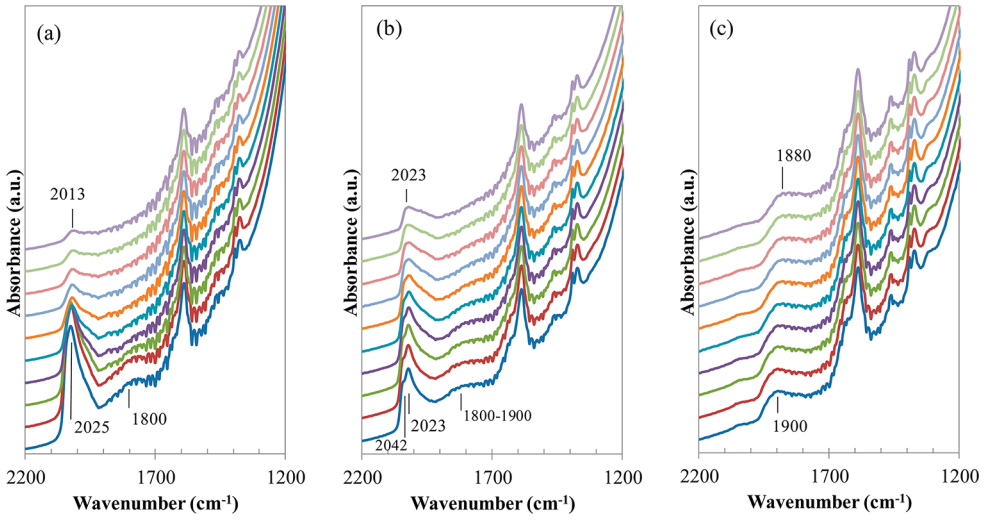

Figure 7. DRIFTS results in transient mode. Spectra recorded after changing from CO_2 (2 mL/min) + H_2 (8 mL/min) + He (10 mL/min) to H_2 (8 mL/min) + He (10 mL/min) flow. Temperature = 175 °C. Samples: (a) Rh100, (b) Rh50−Pd50 , (c) Pd100. From bottom to top: steady state, 1, 5, 10, 15, 20, 25, 30, 35, 40, 45 min after gas switching.

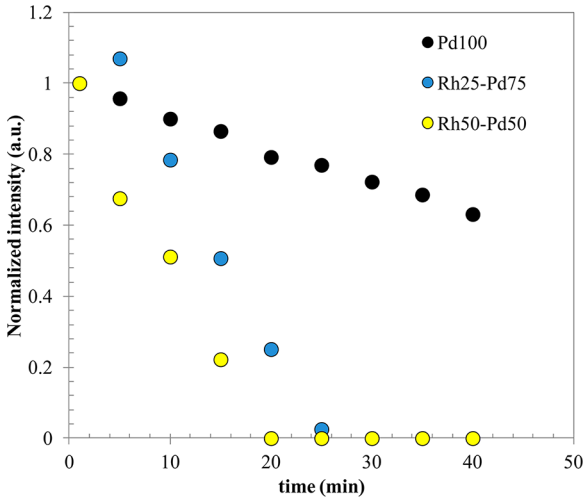

Figure 8. DRIFTS results. Integrated intensity of bridged Pd−CO peak as a function of time in transient experiments at 175 °C. Peak intensity was normalized by the area of the peak right before the transient experiment. At time = 0 min, the gas flow was changed from CO_2 (2 mL/min) + H_2 (8 mL/min) + He (10 mL/min) to H_2 (8 mL/min) + He (10 mL/min).

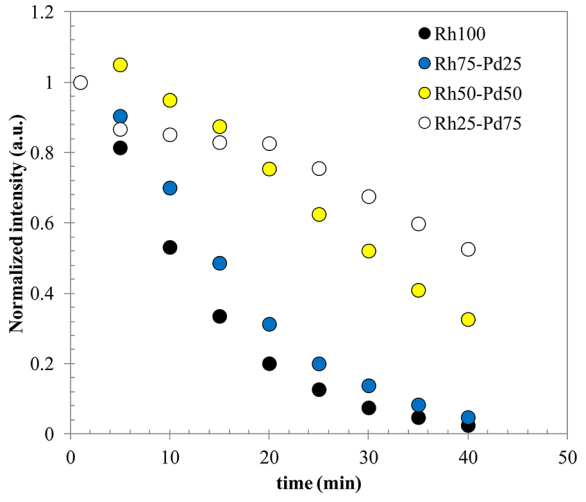

Figure 9. DRIFTS results. Integrated intensity of the linear Rh−CO peak as a function of time in transient experiments at 175 °C. Peak intensity was normalized using the area of the peak right before the transient experiment. At time = 0 min, the gas flow was changed from CO_2 (2 mL/min) + H_2 (8 mL/min) + He (10 mL/min) to H_2 (8 mL/min) + He (10 mL/min).

(Table 4), it is observed that the binding energy of $Pd3d_{5/2}$ electrons and the full width at half-maximum (fwhm) of the peak do not change significantly, showing that after reaction, the electronic state of Pd has not changed appreciably and corresponds to Pd^0. The slight augmentation of binding energy with decreasing Pd content is also observed here. On the basis of the fact that this is observed for fresh and spent catalysts, we ascribe this variation to a weak charging effect induced by the $Rh/\gamma\text{-}Al_2O_3$ catalyst, which would also explain the higher fwhm of $Pd3d_{5/2}$ peak observed for catalysts containing a higher amount of $Rh/\gamma\text{-}Al_2O_3$.

In the case of Rh, because the preparation of $Rh/\gamma\text{-}Al_2O_3$ catalyst included a calcination step, the state of Rh before reaction corresponds to Rh_2O_3 oxide, with $Rh3d_{5/2}$ binding energies between 309.5 and 309.7 eV (Table 3). Catalysts analyzed after reaction show two peaks characteristic of metallic (307.3 eV) and Rh^{3+} species (309 eV). All the samples contain similar amounts of the two species, which suggests that there are no significant changes in the Rh oxidation state after reaction and that the presence of Pd does not affect this property. On the other hand, it has been shown that the reduction of Rh oxides on $\gamma\text{-}Al_2O_3$ is complete at temperatures lower than 200 °C in the case of catalysts with a similar Rh loading and subjected to similar calcination temperatures.[46] This suggests that Rh^{3+} species observed in the case of spent catalysts could arise from the exposure to air of the samples after reaction.

The surface concentration of Pd and Rh measured by XPS is shown in Table 5. In the case of Rh100 catalyst, the Rh/Al XPS ratio is higher than the bulk ratio (Rh/Al = 0.0101). This could be explained by a heterogeneous distribution of Rh particles in the catalyst, which are concentrated on the external surface.[47] The Rh/Al and Pd/Al ratios show a decrease when comparing fresh and spent catalysts. This indicates that some sintering is

dx.doi.org/10.1021/cs400576w | ACS Catal. 2013, 3, 2799−2812

occurring during reaction. This decrease in metal dispersion does not show trends as a function of Pd or Rh loading, suggesting that the presence of one metal does not affect the loss in surface concentration of the other. Regarding at Rh/(Pd + Rh) ratios, it is clear that no significant variations are found between fresh and spent catalysts. This suggests that there is no migration of one metal to the surface of the other that can lead to the formation of bimetallic particles. In addition, hydrogen adsorption isotherms of a mixed catalyst such as Rh50−Pd50 (Figure 3c) show the steep increase in hydrogen uptake at ∼4 kPa that is characteristic of the formation of palladium β-hydride. It has been reported that in the case of Rh−Pd alloy catalysts, the formation of Pd β-hydride is suppressed as a result of the existence of bimetallic nanoparticles instead of pure Pd ones.[48] This can be viewed as a suggestion that in this case, pure Pd and Rh nanoparticles are dominant.

4.2. Kinetic Aspects of Pure and Mixed Catalysts. The activity and kinetic parameters of pure Rh/γ-Al_2O_3 catalyst show good agreement with data reported previously for similar catalysts. Solymosi et al.[49] reported a methane production rate normalized by exposed Rh atoms (TOF) of 2×10^{-2} s^{-1}. On the other hand, a rate of 0.33×10^{-2} s^{-1} is obtained by extrapolation from the data presented by Panagiotopoulou et al.[9] The activity presented here for the Rh/γ-Al_2O_3 catalyst lies between these two values (Table 1). The apparent activation energy obtained here (16.4 kcal/mol) agrees with that presented in the literature for Rh/γ-Al_2O_3 catalysts under similar reaction conditions (17,[50] 16.2 kcal/mol[49]). Moreover, the apparent reaction order for CO_2 methanation was 0.55 for H_2 partial pressure dependence and 0.23 for CO_2 partial pressure dependence (Figure 2). Data provided by Solymosi et al.[49] at the same temperature and pressure are 0.61 and 0.26 for H_2 and CO_2 partial pressures, respectively. In the case of pure Pd/γ-Al_2O_3 catalyst, we found that it is inactive at 200 °C. The catalyst showed activity for CH_4 and CO production at temperatures of 250 °C or higher. The apparent activation energy for methane formation was 23.5 kcal/mol, which is appreciably higher than in the case of the Rh/Al_2O_3 catalyst. Other authors have found activation energies for Pd/Al_2O_3 in CO_2 methanation ranging from 15.5[9] to 23.3 kcal/mol.[14] The differences in activation energies could arise from different dispersions of the metallic phase, as was shown for Rh-based catalysts in CO_2 methanation. Catalysts that differ only in metal dispersion present significantly different apparent activation energies. This has been found for Rh/γ-Al_2O_3[6] and Rh/TiO_2[12] catalysts. If one extrapolates the activity data for Pd/γ-Al_2O_3 collected at 250−350 to 200 °C using the activation energy shown in Table 1, a turnover frequency for CH_4 production of 3.1×10^{-5} s^{-1} is obtained, which is 2 orders of magnitude lower than that obtained for the pure Rh/γ-Al_2O_3 catalyst (Table 1).

The apparent reaction orders for CO_2 methanation over Pd/γ-Al_2O_3 obtained at 300 °C are 0.81 for H_2 partial pressure dependence and −0.09 for CO_2 partial pressure dependence. Compared with the Rh/γ-Al_2O_3 catalyst, the H_2 apparent reaction order is significantly higher (0.81 vs 0.55). In the case of the CO_2 apparent reaction order, the Pd/γ-Al_2O_3 catalyst presents a considerably lower reaction order of −0.09 vs 0.23 for Rh/γ-Al_2O_3. If it is assumed that the mechanism of reaction is similar for Rh- and Pd-based catalysts, a comparison of the two catalysts can be made in terms of concentration and strength of adsorption of surface species. It has been proposed that the mechanism of reaction over Rh proceeds by the surface reaction of H(ads) and CO(ads) species (the latter coming from CO_2 dissociation on the metal surface) to form a hydrogenated CO intermediate that is subsequently hydrogenated to methane.[12,22] The higher reaction order with respect to H_2 and the lower CO_2 reaction order found for Pd/γ-Al_2O_3 compared with Rh/γ-Al_2O_3 indicates that on the former, the coverage of CO(ads) species predominates over H(ads) species. In the case of Rh/γ-Al_2O_3, the adsorption energy of CO(ads) would be lower, and hence, a lower coverage of CO(ads) species could be expected.

Figure 10 shows the reaction orders for pure catalysts and mechanical mixtures with respect to H_2 and CO_2 as a function

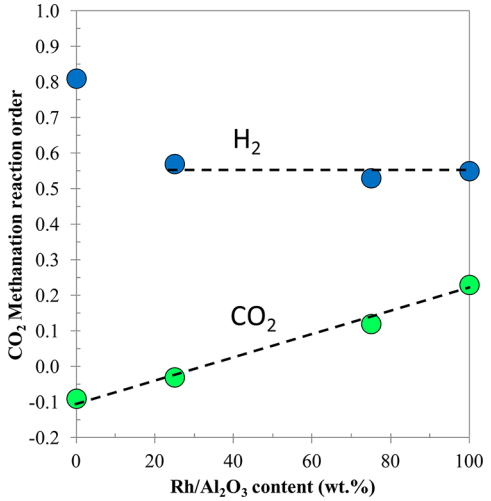

Figure 10. Apparent CO_2 and H_2 reaction order in CO_2 methanation reaction at 200 °C as a function of Rh/Al_2O_3 content. (Data were obtained at 300 °C for the Pd100 catalyst; Rh/Al_2O_3 content = 0 wt %.)

of Rh/γ-Al_2O_3 content. When the Rh/γ-Al_2O_3 catalyst is modified by addition of Pd/γ-Al_2O_3, the reaction order with respect to H_2 does not change, being approximately 0.53−0.57 for all the mixtures analyzed. On the other hand, the CO_2 reaction order decreases linearly from 0.23 for Rh100 to −0.09 for Pd100. These results strongly suggest that for mechanical mixtures, the sites responsible for H_2 activation are located on Rh/γ-Al_2O_3 because the H_2 partial pressure dependence is that found over the pure Rh/γ-Al_2O_3 catalyst. The continuous decrease in the CO_2 reaction order with the addition of Pd/γ-Al_2O_3 on the mixtures, and thus approaching the CO_2 reaction order for pure Pd/γ-Al_2O_3, suggests that new sites responsible for CO_2 activation and methane production are being created on Pd/γ-Al_2O_3 in addition to those already existing on Rh/γ-Al_2O_3. Regarding the apparent activation energies (Table 1), a continuous increase is observed, from 16.3 kcal/mol in the case of Rh100 to 21.6 and 21.1 kcal/mol for Rh50−Pd50 and Rh25−Pd75 mechanical mixtures, respectively. As the activation energy increases with an increment in the content of Pd/γ-Al_2O_3, the maximum in activity is affected by the temperature. It shifts from Rh90−Pd10 at 150 °C to Rh50−Pd50 at 200 °C (Figure 1b). As the Pd/γ-Al_2O_3 content is increased, the activation energies of the mixtures approach that of pure Pd/γ-Al_2O_3 catalyst (23.5 kcal/mol). According to this result, it can be suggested that when Pd/γ-Al_2O_3 is added, the reaction starts to take place on the Pd/γ-Al_2O_3 catalyst, since the apparent activation energy approaches steadily that of pure

dx.doi.org/10.1021/cs400576w | ACS Catal. 2013, 3, 2799−2812

Pd/γ-Al_2O_3. This agrees well with the observed continuous decrease in CO_2 reaction order with Pd/γ-Al_2O_3 addition.

4.3. Surface Species. Figure 4a shows the spectra recorded at steady state over the Rh100 catalyst at different temperatures under a CO_2 + H_2 flow. The peak appearing at 50 °C at 2046 cm^{-1} is assigned to CO species adsorbed linearly on Rh. The mechanism of Rh−CO formation from CO_2 has been suggested to proceed by the dissociation of CO_2 to CO(ads) and O(ads).[5,12,24,51] Another mechanism, in which CO(ads) formation proceeds by the water-gas shift reaction on the surface with formate as a reaction intermediate, has also been proposed in the literature.[52−55]

In the present work, the absence of formate species (1393 cm^{-1}) at 50 °C and the fact that at these low temperatures water-gas shift reaction does not occur suggest that CO(ads) is formed by dissociation of CO_2 on Rh. When the temperature is raised, the peak associated with linear Rh−CO species (2046 cm^{-1}) increases appreciably in intensity and shifts to lower wavenumbers. Normally, an increase in CO(ads) coverage would lead to a shift of the Rh−CO band to higher wavenumbers as a result of an increase in dipole−dipole coupling of CO(ads) species.[56] The inverse phenomenon is observed here. This has been explained by the gradual formation of Rh carbonyl hydride species when the temperature is increased. Rh carbonyl hydrides are formed by a CO molecule linearly adsorbed to Rh onto which one or two H atoms are coadsorbed.[36,57] The H atom bound to Rh is electron-donating, which increases the π-donation from Rh to the antibonding π orbital of CO, thus decreasing the frequency of CO(ads) stretching.[36] Another explanation involves a geometric effect, namely, the H atom uncouples the dipole−dipole interaction of the CO(ads) species, leading to a shift of the CO(ads) band to lower wavenumbers.[45] Rh carbonyl hydride species have been invoked to explain the absence of gem-dicarbonyl species on Rh when the gas phase contains CO_2 + H_2 instead of CO + H_2 mixtures.[13,58]

In the case of the Pd100 catalyst (Figure 4c), dissociation of CO_2 is more difficult. CO(ads) coming from CO_2 dissociation are observed only at temperatures of 150 °C or higher. As in the case of the Rh100 catalyst, the appearance of CO(ads) species occurs before CH_4 is detected in the gas phase, which suggests that CO_2 dissociation is facile compared with the activation of CO(ads) species. The dissociation of such CO(ads) has been proposed to be the rate-determining step in the CO_2 methanation reaction.[8,22−24] The formation of bridged CO(ads) species takes place at 150 °C, with a peak at 1860 cm^{-1}. Linearly adsorbed CO species are absent from this catalyst. Other authors have also found that linearly bonded CO is absent when the gas phase is composed of CO_2 + H_2 instead of pure CO.[45] It was proposed that the formation of CO(ads) by CO_2 dissociation requires an ensemble of surface Pd atoms. Increasing the temperature to 200 °C leads to a shift to higher wavenumbers (1900 cm^{-1}) and an increase in the peak intensity, which means that the rate of CO_2 dissociation is enhanced with temperature, leading to a higher coverage of CO(ads) species. The shift to higher wavenumbers can be explained by an increment in dipole−dipole interaction between CO(ads) species due to a higher coverage. The presence of Pd carbonyl hydrides over Pd/γ-Al_2O_3 cannot be confirmed because one of the characteristic features of such peaks, the shift in the opposite direction with an increase in coverage, is not observed; however, the position at which the bridged Pd−CO species appear (1900 cm^{-1}) is lower than that observed when CO instead of CO_2 is used for the adsorptions (1950−1970 cm^{-1}).[45] This suggests that Pd carbonyl hydride could be formed on the Pd surface. The intensity of the formate band (1393 cm^{-1}) is higher in the case of the Pd100 catalyst compared with Rh100. This can be related to the higher surface area of the former (Table 2) and, thus, a larger number of surface sites capable of accommodating formates.

In the case of the Rh50−Pd50 mechanical mixture (Figure 4b), the peak associated with the Rh−CO species behaves similarly when compared with the Rh100 catalyst. The main difference is the existence of two peaks in that region. The peak at 2023 cm^{-1} can be associated with Rh carbonyl hydrides, and that at 2042 cm^{-1}, with linear Rh−CO species, without association with H atoms. Figure 5 shows that the simultaneous existence of these two species occurs for the Rh50−Pd50 and also for the Rh25−Pd75 catalyst. Catalysts with higher Rh/γ-Al_2O_3 loading show predominantly Rh carbonyl hydride species (Rh100 and Rh75−Pd25).

The decomposition of the different CO(ads) species on Rh can be used to estimate the relative contribution of linear relative to bridged species. According to the data presented by Duncan et al.,[59] the integrated adsorption coefficients (A_i) for CO adsorbed in linear form over Rh/Al_2O_3 are A_l = 11.3 cm/μmol and, for the bridged form on the same catalyst, A_b = 36.9 cm/μmol. If we assume that the coefficient for linear Rh−CO in carbonyl hydride form can be approximated using that for Rh−CO species, the relative contributions of linear and bridged CO species can be calculated by dividing the area of the peak by the respective A_i. For the Rh100 catalyst, 95% of the CO absorbed species are in linear form. Taking into account this result, we can safely assume that the predominant Rh−CO species are those adsorbed in linear form, and hence, they will be used to study the reactivity of CO adsorbed on Rh.

Figure 6 shows the area of the band associated with Rh−CO in linear form as a function of temperature at steady state reaction conditions. The areas were normalized by the amount of Rh in the catalysts. Up to 150 °C, no significant differences in coverage of Rh−CO species exist among the catalysts. This means that the coverage of CO(ads) on Rh seems to be unaffected by the presence of the Pd/γ-Al_2O_3 catalyst in the vicinity. However, when the temperature is increased to 200 °C, the evolution of the coverage of Rh−CO species seems to depend on the amount of Rh. Catalysts with higher amounts of Rh, such as for Rh100 and Rh75−Pd25, present a decrease or stabilization of the amount of CO(ads) on Rh, whereas catalysts with less Rh, such as Rh50−Pd50 and Rh25−Pd75, show an increase in the amount of the Rh−CO species.

In the case of the Pd−CO species, a reliable comparison of the relative quantities of this species among the different catalysts cannot be made with the available results because the peak of the Pd−CO species overlaps with that of the bridged Rh−CO. However, as will be discussed below, the dynamics of the different peaks, including that of Pd−CO, can give important insights into the synergic mechanism.

4.4. Dynamic Phenomena on the Catalyst Surface. Figure 7 shows the dynamic behavior of observable surface species when exposed to hydrogen at 175 °C. In the case of the Rh100 catalyst (Figure 7a), the peak at 2025 cm^{-1}, which has been attributed to Rh carbonyl hydride species, presents a shift to lower wavenumbers, and its intensity decreases with time. The shift to lower wavenumbers can be explained by a decrease in dipole−dipole coupling due to a decrease in CO(ads) coverage. For the Rh50−Pd50 catalyst, the region where Rh−

dx.doi.org/10.1021/cs400576w | ACS Catal. 2013, 3, 2799−2812

CO species appear presents two clear peaks: the peak at 2023 cm^{-1} was assigned to Rh carbonyl hydrides, whereas that the one at 2042 cm^{-1} was proposed to arise from linear Rh−CO species without association with H atoms. The presence of Rh−CO species in addition to Rh carbonyl hydrides in the case of Rh50−Pd50 and Rh25−Pd75 (Figure 5) suggests that there are fewer H species available to react with the CO(ads) species adsorbed on the Rh on these catalysts.

Regarding Figure 9, it is observed that after 40 min in H_2, the Rh carbonyl band of the Rh50−Pd50 catalyst showed a decrease that is equivalent to that shown by Rh100 after only 15 min, which indicates that Rh−CO species adsorbed on mechanical mixtures with high Pd/γ-Al_2O_3 loading are less reactive than those on catalysts where Rh/γ-Al_2O_3 predominates. The position of the bands at these reaction times is different. For Rh100, after 15 min, the band is located at 2020 cm^{-1}, whereas for a similar decrease in intensity, the band of Rh50−Pd50 appears at 2023 cm^{-1} and that after 40 min in H_2 (Figure 7 and Figure 9). This observation suggests that over catalysts containing a higher proportion of Pd/γ-Al_2O_3, non-hydrogenated Rh−CO species are present in higher amounts than over Rh-rich catalysts in which the majority of Rh−CO species are forming Rh carbonyl hydrides. This means that the addition of Pd leads to a decrease in the amount of hydrogen available to hydrogenate Rh−CO to form Rh carbonyl hydrides.

Concerning the role of formates and carbonates in the reaction mechanism, in Figure 7, it is observed that these bands (appearing at wavenumbers <1700 cm^{-1}) do not change appreciably under hydrogen flow, implying that their reactivity is not significant under the applied conditions. This agrees with previous results, which propose that formates are spectators in the CO_2 methanation reaction.[6,12,13,51]

The reactivity of Rh−CO species in hydrogen at 175 °C for all the catalysts is presented in Figure 9. All the peaks arising from linear Rh−CO species were added. Because it was demonstrated that linear CO species account for more than 95% of the CO species adsorbed on Rh (the others being bridged Rh−CO species) their evolution can be considered representative of all Rh−CO species. The reactivity of Rh−CO species is enhanced for catalysts containing a larger proportion of Rh (Rh100 and Rh75−Pd25). In contrast, catalysts with a lower Rh content, such as Rh50−Pd50 and Rh25−Pd75, show a clear decrease in the Rh−CO reactivity.

Figure 8 shows the evolution of Pd−CO species when exposed to hydrogen at 175 °C. It is clearly seen that CO species adsorbed on Pd, which are not reactive when the catalyst contains only Pd, become reactive when Rh/γ-Al_2O_3 is present in the catalyst. The reactivity of surface CO species adsorbed on Pd could be invoked to explain the observed synergistic effect. The fact that Pd−CO species are participating in the mechanism and give rise to methane agrees well with an increase in the apparent activation energy (from 16.4 to 21.6 kcal/mol) of Rh/γ-Al_2O_3 + Pd/γ-Al_2O_3 mixtures that approaches that of pure the Pd/γ-Al_2O_3 catalyst. In addition, the apparent CO_2 reaction orders of Rh/γ-Al_2O_3 + Pd/γ-Al_2O_3 catalysts linearly approach the value of the pure Pd/γ-Al_2O_3 catalyst when the Pd content is increased (Figure 10), which is another indication that CO species on Pd (which would arise from CO_2 dissociated on Pd/γ-Al_2O_3) give rise to methane.

The reasons for the higher synergistic effect observed for Rh75−Pd25 catalyst compared with catalysts containing more Pd/γ-Al_2O_3, such as Rh25−Pd75, is another issue that needs explanation. Regarding Figure 8, it is clear that the addition of Pd/γ-Al_2O_3 decreases the reactivity of the Rh−CO species toward hydrogen. It can be suggested that a transfer of H species occurs from Rh to Pd, leading to a decrease in the reactivity of the Rh−CO species. It was shown that over catalysts that are rich in Pd/γ-Al_2O_3, such as Rh25−Pd75 and Rh50−Pd50, there is the formation of Rh−CO species in addition to Rh carbonyl hydrides (Figure 5), which would be a consequence of a lower amount of H available on Rh/γ-Al_2O_3 over these catalysts. In addition, regarding the apparent H_2 reaction orders of the mixtures (Figure 10), it is clear that no appreciable change with respect to Rh100 takes place: the order is 0.53−0.57 in all cases. This is a confirmation that under these experimental conditions, Pd/γ-Al_2O_3 is not able to activate hydrogen; otherwise, the Rh−CO hydrogenation rate should have increased when the amount of Pd/γ-Al_2O_3 increased.

It can be suggested that regardless of the proportion of Rh/γ-Al_2O_3 and Pd/γ-Al_2O_3 in the mixtures, the majority of H_2 is activated on Rh and then is available to react with CO(ads) species present on both the Rh/γ-Al_2O_3 and Pd/γ-Al_2O_3 catalysts. For catalysts with a large amount of Pd/γ-Al_2O_3 (e.g., Rh25−Pd75), the activation of CO(ads) predominates on Pd over Rh. In addition, because of the lower intrinsic activity of Pd in methanation, the overall rate is not enhanced and is even decreased with respect to pure Rh100 (Figure 1b). In the case of Rh/γ-Al_2O_3-rich catalysts (e.g., Rh75−Pd25), the reactivity of Rh−CO species is nearly unaffected by the presence of Pd, as is shown in Figure 9. In addition, the decrease in the CO_2 reaction order and the increase in the apparent activation energy, both approaching the values for pure Pd/γ-Al_2O_3, suggest that over Rh/γ-Al_2O_3-rich mixtures, the reaction is also occurring on Pd, which leads to an increase in the overall reaction rate.

Mechanical mixtures presented high selectivity toward methane (100%), whereas pure Pd/γ-Al_2O_3 showed only 60% CH_4 selectivity at 300 °C, the rest being CO. This can be explained by the lower temperature at which the reaction was performed with the mixtures (≤200 °C). Because the production of CO involves the desorption of CO(ads) species, it is suggested that at the low temperatures studied, the desorption is less favored, and thus, the hydrogenation path of CO(ads) species is enhanced, which leads to a higher methane selectivity.

5. CONCLUSIONS

A synergistic effect was found to occur when contacting Pd(5 wt %)/γ-Al_2O_3 and Rh(2 wt %)/γ-Al_2O_3 catalysts by simple mechanical mixing in CO_2 methanation at temperatures between 150 and 200 °C. The presence of the Pd/γ-Al_2O_3 catalyst (which itself is not active under these experimental conditions) permits an increase in the reaction rate at 200 °C from 0.218 × 10^{-2} $mol_{CH_4}/mol_{Rh}/s$ for the pure Rh/γ-Al_2O_3 catalyst to 0.318 × 10^{-2} $mol_{CH_4}/mol_{Rh}/s$ for a catalyst containing 50 wt % of each catalyst. Physicochemical characterization shows that there are no significant differences in the oxidation state of Rh or Pd when comparing mono- and bimetallic catalysts. No indication of migration of one metal to the surface of the other that can lead to the formation of bimetallic structures in the mixtures was observed. The apparent activation energies and reaction orders (with respect to CO_2 and H_2) reveal that for mechanical mixtures, H_2 is essentially activated over Rh/γ-Al_2O_3, but the activation of CO_2

and its dissociation with CO(ads) and subsequent hydrogenation to methane can take place on both Pd/γ-Al_2O_3 and Rh/γ-Al_2O_3. The negative CO_2 reaction order (−0.09) and the higher H_2 reaction order (0.81) found for pure Pd/γ-Al_2O_3 (at 300 °C) suggest that over this catalyst, CO(ads) species are too strongly adsorbed, and the reaction is slow. The presence of Rh/γ-Al_2O_3 facilitates the activation of H_2, and thus, H species are able to migrate and react with CO(ads) on Pd/γ-Al_2O_3, leading to selective methane formation (no CO was observed). Pd−CO intermediates are active only when the Rh/γ-Al_2O_3 is present in the catalyst mixture, which explains the observed synergistic effect. It is proposed that Rh carbonyl hydride is the main form of CO adsorption over the Rh/Al_2O_3 catalyst. In the case of mechanical mixtures, the presence of both linear Rh−CO species and Rh carbonyl hydride shows that less H is available as a result of its reaction with Pd−CO intermediates. The results provide evidence that help in the understanding of the synergistic effects operating in bimetallic catalysts in CO_2 hydrogenation reactions. It is shown that a synergy, via hydrogen migration, can operate at temperatures as low as 150 °C. The preparation of catalysts in which Pd and Rh are intimately mixed could be envisaged to increase this synergistic effect even more.

AUTHOR INFORMATION

Corresponding Author

*Phone: +32 010473651. E-mail: alejandro.karelovic@uclouvain.be.

Notes

The authors declare no competing financial interest.

ACKNOWLEDGMENTS

The authors gratefully acknowledge the Direction Générale des Technologies, de la Recherche et de l'Energie (DGTRE) of the Région Wallonne (Belgium) and the Fonds National de la Recherche Scientifique (FNRS) of Belgium for their financial support. The involvement of IMCN-MOST in the INANOMAT IUAP network sustained by the Service public fédéral de programmation politique scientifique (Belgium) is acknowledged. The authors are grateful to Michel J. Genet for his valuable help in adapting CasaXPS for treating infrared spectra. A.K. acknowledges the Becas Chile program of CONICYT (Chile) for a Ph.D. grant.

REFERENCES

(1) Somorjai, G. A.; Rioux, R. M. *Catal. Today* **2005**, *100*, 201−215.
(2) Aresta, M.; Dibenedetto, A. *Dalton Trans.* **2007**, 2975−2992.
(3) Centi, G.; Perathoner, S. *Catal. Today* **2009**, *148*, 191−205.
(4) Centi, G.; Perathoner, S. *Greenhouse Gases Sci. Technol.* **2011**, *1*, 21−35.
(5) Beuls, A.; Swalus, C.; Jacquemin, M.; Heyen, G.; Karelovic, A.; Ruiz, P. *Appl. Catal., B* **2012**, *113−114*, 2−10.
(6) Karelovic, A.; Ruiz, P. *Appl. Catal., B* **2012**, *113−114*, 237−249.
(7) Abe, T.; Tanizawa, M.; Watanabe, K.; Taguchi, A. *Energy Environ. Sci.* **2009**, *2*, 315−321.
(8) Prairie, M. R.; Renken, A.; Highfield, J. G.; Ravindranathan Thampi, K.; Grätzel, M. *J. Catal.* **1991**, *129*, 130−144.
(9) Panagiotopoulou, P.; Kondarides, D. I.; Verykios, X. E. *Appl. Catal., A* **2008**, *344*, 45−54.
(10) Melsheimer, J.; Guo, W.; Ziegler, D.; Wesemann, M.; Schlogl, R. *Catal. Lett.* **1991**, *11*, 157−168.
(11) Jacquemin, M.; Beuls, A.; Ruiz, P. *Catal. Today* **2010**, *157*, 462−466.
(12) Karelovic, A.; Ruiz, P. *J. Catal.* **2013**, *301*, 141−153.
(13) Solymosi, F.; Pasztor, M. *J. Catal.* **1987**, *104*, 312−322.
(14) Erdohelyi, A.; Pasztor, M.; Solymosi, F. *J. Catal.* **1986**, *98*, 166−177.
(15) McFarland, E. W.; Park, J. N. *J. Catal.* **2009**, *266*, 92−97.
(16) Araya, P.; Díaz, V. *J. Chem. Soc., Faraday Trans.* **1997**, *93*, 3887−3891.
(17) Sheng, P. Y.; Chiu, W. W.; Yee, A.; Morrison, S. J.; Idriss, H. *Catal. Today* **2007**, *129*, 313−321.
(18) Ogihara, H.; Takenaka, S.; Yamanaka, I.; Tanabe, E.; Genseki, A.; Otsuka, K. *J. Catal.* **2006**, *238*, 353−360.
(19) Ersson, A.; Kušar, H.; Carroni, R.; Griffin, T.; Järås, S. *Catal. Today* **2003**, *83*, 265−277.
(20) Christensen, C. H.; Sehested, J.; Larsen, K. E.; Kustov, A. L.; Frey, A. M.; Johannessen, T.; Bligaard, T.; Andersson, M. P.; Norskov, J. K. *Top. Catal.* **2007**, *45*, 9−13.
(21) Swalus, C.; Jacquemin, M.; Poleunis, C.; Bertrand, P.; Ruiz, P. *Appl. Catal., B* **2012**, *125*, 41−50.
(22) Williams, K. J.; Boffa, A. B.; Salmeron, M.; Bell, A. T.; Somorjai, G. A. *Catal. Lett.* **1991**, *9*, 415−426.
(23) Weatherbee, G. D.; Bartholomew, C. H. *J. Catal.* **1982**, *77*, 460−472.
(24) Fisher, I. A.; Bell, A. T. *J. Catal.* **1996**, *162*, 54−65.
(25) Force, C.; Ruiz Paniego, A.; Guil, J. M.; Gatica, J. M.; López-Cartes, C.; Bernal, S.; Sanz, J. *Langmuir* **2001**, *17*, 2720−2726.
(26) Chou, P.; Vannice, M. A. *J. Catal.* **1987**, *104*, 1−16.
(27) Sirita, J.; Phanichphant, S.; Meunier, F. C. *Anal. Chem.* **2007**, *79*, 3912−3918.
(28) Bollmann, L.; Ratts, J. L.; Joshi, A. M.; Williams, W. D.; Pazmino, J.; Joshi, Y. V.; Miller, J. T.; Kropf, A. J.; Delgass, W. N.; Ribeiro, F. H. *J. Catal.* **2008**, *257*, 43−54.
(29) Vannice, M. A. *Kinetics of Catalytic Reactions*; Springer: New York, 2005; p 240.
(30) Benson, J. E.; Hwang, H. S.; Boudart, M. *J. Catal.* **1973**, *30*, 146−153.
(31) Brun, M.; Berthet, A.; Bertolini, J. C. *J. Electron Spectrosc. Relat. Phenom.* **1999**, *104*, 55−60.
(32) Wagner, C. D.; Riggs, W. M.; Davis, L. E.; Moulder, J. F. *Handbook of X-ray Photoelectron Spectroscopy*; Perkin-Elmer Corporation, Physical Electronics Division: Eden Prairie, MN, 1979.
(33) Kawai, M.; Uda, M.; Ichikawa, M. *J. Phys. Chem.* **1985**, *89*, 1654−1656.
(34) Brinen, J. S.; Melera, A. *J. Phys. Chem.* **1972**, *76*, 2525−2526.
(35) Yang, C.; Garl, C. W. *J. Phys. Chem.* **1957**, *61*, 1504−1512.
(36) Solymosi, F.; Erdohelyi, A.; Kocsis, M. *J. Catal.* **1980**, *65*, 428−436.
(37) Lavalley, J. C.; Saussey, J.; Lamotte, J.; Breault, R.; Hindermann, J. P.; Kiennemann, A. *J. Phys. Chem.* **1990**, *94*, 5941−5947.
(38) Rege, S. U.; Yang, R. T. *Chem. Eng. Sci.* **2001**, *56*, 3781−3796.
(39) Betta, R. A. D.; Shelef, M. *J. Catal.* **1977**, *48*, 111−119.
(40) Wijnja, H.; Schulthess, C. P. *Spectrochim. Acta A* **1999**, *55*, 861−872.
(41) Busca, G.; Lorenzelli, V. *Mater. Chem.* **1982**, *7*, 89−126.
(42) Solymosi, F.; Erdohelyi, A.; Bansagi, T. *J. Chem. Soc., Faraday Trans. 1* **1981**, *77*, 2645−2657.
(43) Chuang, S. S. C.; Stevens, R. W.; Khatri, R. *Top. Catal.* **2005**, *32*, 225−232.
(44) Sachtler, W. M. H.; Ichikawa, M. *J. Phys. Chem.* **1986**, *90*, 4752−4758.
(45) Solymosi, F.; Erdohelyi, A.; Lancz, M. *J. Catal.* **1985**, *95*, 567−577.
(46) Hwang, C. P.; Yeh, C. T.; Zhu, Q. M. *Catal. Today* **1999**, *51*, 93−101.
(47) Cimino, A.; Gazzoli, D.; Valigi, M. *J. Electron Spectrosc. Relat. Phenom.* **1999**, *104*, 1−29.
(48) Holles, J. H.; Switzer, M. A.; Davis, R. J. *J. Catal.* **2000**, *190*, 247−260.
(49) Solymosi, F.; Erdohelyi, A.; Bansagi, T. *J. Catal.* **1981**, *68*, 371−382.
(50) Iizuka, T.; Tanaka, Y.; Tanabe, K. *J. Catal.* **1982**, *76*, 1−8.

(51) Eckle, S.; Anfang, H.-G.; Behm, R. J. *J. Phys. Chem. C* **2010**, *115*, 1361−1367.
(52) Marwood, M.; Doepper, R.; Renken, A. *Appl. Catal., A* **1997**, *151*, 223−246.
(53) Kondarides, D. I.; Panagiotopoulou, P.; Verykios, X. E. *J. Phys. Chem. C* **2011**, *115*, 1220−1230.
(54) Panagiotopoulou, P.; Kondarides, D. I.; Verykios, X. E. *Catal. Today* **2012**, *181*, 138−147.
(55) Schild, C.; Wokaun, A.; Koeppel, R. A.; Baiker, A. *J. Phys. Chem.* **1991**, *95*, 6341−6346.
(56) Niemantsverdriet, J. W. *Spectroscopy in Catalysis*; Wiley-VCH: Weinheim, 2007.
(57) Henderson, M. A.; Worley, S. D. *Surf. Sci.* **1985**, *149*, L1−L6.
(58) Henderson, M. A.; Worley, S. D. *J. Phys. Chem.* **1985**, *89*, 392−394.
(59) Duncan, T. M.; Yates, J. T.; Vaughan, R. W. *J. Chem. Phys.* **1980**, *73*, 975−985.